Novel composite photocatalyst made of TiO$_2$ nanoparticles

A. Vega, G. E. Imoberdorf, M. Keshmir and M. Mohseni

ABSTRACT

A novel photocatalyst based on TiO$_2$ nanoparticles was developed for application in fluidised bed photocatalytic reactors for water treatment. The mechanically robust photocatalyst consists of composite spheres made of TiO$_2$ nanoparticles and TiO$_2$ commercial powder. X-ray diffraction (XRD), scanning electron microscopy (SEM) and specific surface area analysis (BET) were used to characterise the catalyst. The photocatalytic activity was evaluated using model pesticide micro-pollutant. A complete model comprised of radiation, kinetic, and reactor bed models was also developed, allowing for detailed analysis of the photoreactor.

Key words | fluidised bed photocatalytic reactor, modelling, organic pollutant, sol–gel method, TiO$_2$ nanoparticles

A. Vega
G. E. Imoberdorf
M. Keshmir
M. Mohseni
Department of Chemical and Biological
Engineering,
University of British Columbia,
2360 East Mall,
Vancouver BC V6T 1Z3,
Canada
E-mail: *mmohseni@chml.ubc.ca*

INTRODUCTION

Nanoparticles of titanium dioxide (TiO$_2$) are proven to be effective photocatalysts for contaminant removal from drinking water (Bassekhouad *et al.* 2003). In a photocatalytic process, organic pollutants are mineralised or partially degraded to smaller and non-toxic species, once they interact with the photogenerated electron-holes on the UV-irradiated TiO$_2$ catalyst surface (Herrmann 1999).

Films of TiO$_2$ nanoparticles have been immobilised on different inert supports, such as zeolite pellets, glass spheres, quartz wool, optical fibres, and on reactor walls. However, two problems have been found: i) the effectiveness of the process is highly reduced by diffusive mass resistances, and ii) the activity of the photocatalyst decays with time because the TiO$_2$ nanoparticles are gradually detached due to attrition leading to an increased overall cost of the process due to filtration (Nelson *et al.* 2007).

Heterogeneous catalysts, such as TiO$_2$, are often prepared by wet chemistry methods such as precipitation, coprecipitation, hydrothermal synthesis or Sol–Gel process (Campanati *et al.* 2003). The sol–gel (solution–gelation) process, which is mainly based on inorganic polymerisation reactions, is defined as a sequence of chemical synthesis method initially used for the preparation of inorganic materials such as glasses and ceramics (Wen & Wilkes 1996). Currently, sol–gel is one of the most common techniques for preparing nanosized metallic oxide materials with high photocatalytic activities (Su *et al.* 2004). In the last decades, the application of sol–gel process to produce photoactive materials has been explored because of the advantages of this process compared to other methods. For example, the low temperature requirement gives solids large specific surface area and high porosity in the meso- and macro-pore ranges (Livage 1998).

During the sol–gel process, hydrolysis and condensation reactions are known as key steps. Controlling these reactions of the precursor, usually a metal alkoxide, with water will produce a three dimensional network structure in the form of a gel. Then, with the subsequent drying and calcination steps, the structure may result in an oxide structure.

In this research, sol–gel principles were applied to produce a liquid phase sol of TiO$_2$ nanoparticles, which were used to produce template–free spheres with a considerable degree of consistency in their size and shape.

These nanoparticles helped to bond together commercial TiO$_2$ precalcined powder by the assistance of a polymeric structure formed upon fast gelation of this material when it was in contact with aqueous solutions. Synthesis variables such as reactant concentrations, pH, viscosity, and sintering temperature were studied in order to maximise the photocatalytic activity and to reduce the attrition effect.

In order to study the photocatalytic activity, a model for the fluidised bed photoreactor was developed. A Langmuir–Hinshelwood model was used to describe the degradation kinetics of a model pollutant (pesticide 2,4 D). To describe the propagation of radiation in the reactor, a bed model based on stochastic rules was coupled to a radiation model, which was solved using the Monte Carlo method (Imoberdorf *et al.* 2008).

EXPERIMENTAL

Photocatalyst preparation

In the preparation steps of the sol–gel derived composite TiO$_2$ spheres, denatured alcohol is used as a solvent to prevent fast hydrolysis of titanium alkoxide. Water is added to the alcohol followed by the catalyst, in this case HCl, which is used to prevent fast gelation of the sol, control the rate of condensation, and eliminate the possibility of precipitate formation due to uncontrolled hydrolysis reaction. Then, titanium alkoxide is added as a precursor followed by the pre-calcined commercial TiO$_2$ powder that is used as a filler material. Good agitation is required to dissolve the powder into the solution and create a homogeneous solution called Composite Sol–Gel (CSG).

The CSG is then mixed with a polymeric matrix to create a solution with the desired viscosity needed for sphere formation. This solution is added drop-wise into a basic solution to produce the TiO$_2$ spheres due to fast gelation of the CSG–polymer matrix in basic pH (NH$_4$OH solution in this case). Finally, the drying process and the heat treatment are necessary to induce the final crystallographic structure in the catalyst. For this study, the spheres were dried at 80°C for 21 h followed by a heat treatment at 600°C for 3 h. This temperature–time relation is sufficient for the bond formation, ensuring the desired structure of the spheres with high photoactivity and good attrition resistance.

Experimental setup and procedure

The experimental setup consisted of a tubular photoreactor that was coupled with a centrifugal pump, a storage tank, and connecting tubing, allowing for the recirculation of water through the reactor (Figure 1). The photoreactor was made of quartz, with a tubular configuration. The photocatalyst consisted of 25 g of CSG TiO$_2$ spheres. Three UV–Hg lamps (254 nm output, GPH357T5L/4P, Light Sources Inc.) were longitudinally placed surrounding the reactor. The distance of the lamps to the reactor was modified to change the radiation flux reaching the reactor. The storage tank was equipped with a porous diffuser, sparging air through the solution. For each experimental run, a volume of 500 cm^3 of milli-Q water with different concentration of a model pesticide pollutant, 2,4-Dichlorophenoxyacetic acid (2,4 D), was treated in the photoreactor. The recycling flow rate was relatively high (3,400 cm^3/min), and the bed expansion of the TiO$_2$ was 435%.

Analytical methods

Method to determine the attrition in the system

The attrition in this system was determined using an analytical technique reported elsewhere (Eisenberg 1943;
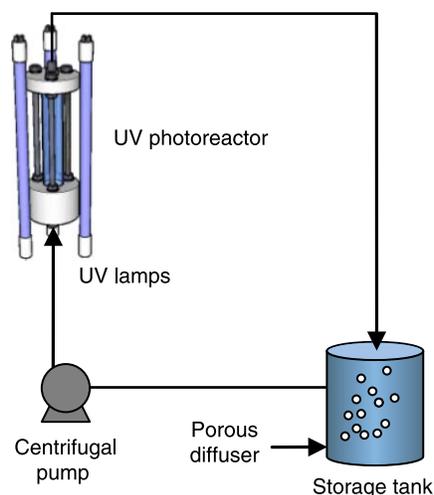

Figure 1 | Experimental setup.

Jackson 1883). In this technique, a sample of the solution was taken to produce a $Ti(SO_4)_2$ solution that reacted with hydrogen peroxide (H_2O_2) producing a coloured solution. The amount of Ti^{4+} present in the solution was determined using a spectrophotometer (Shimadzu 1240) at $\lambda = 410$ nm.

Photocatalytic activity

Photocatalytic activity of the TiO_2 spheres was evaluated by monitoring the concentration of 2,4 D remaining in the solution over the course of treatment. The concentrations of residual 2,4 D and by-products of its partial photocatalytic oxidation were quantified using a high-performance liquid chromatograph (Waters 2695–HPLC) equipped with C-18 column (4-μm particle diameter) and a UV-detector. Acetonitrile/water/acetic acid (50:50:0.2% v/v) was used as the mobile phase. The flow rate of mobile phase for analysis was kept at 1 mL/min using $\lambda = 280$ nm for UV detection. Reagent grade standards were used to calibrate the HPLC for the parent contaminant and its oxidation by-products.

RESULTS

Photocatalyst characterisation

The shape and size of the CSG TiO_2 spheres were observed using a Scanning Electron Microscope (SEM) at high magnification. The spheres were consistent in size and shape and had an average diameter of 1.15 mm (Figure 2).

Using an X-ray diffractomer (XRD) and Rietveld analysis, the amount of anatase and rutile in the composite photocatalyst was determined. The results indicated that the weight fractions of anatase and rutile were 65% and 35%, respectively. In comparison, the commercial TiO_2 (Degussa P25) has a weight fraction of 88% for anatase and 12% for rutile.

The surface area, pore size distribution, and pore volume of the photocatalyst were obtained by nitrogen adsorption/desorption at 77 K. Composite TiO_2 spheres had a surface area of 29 m²/g, which is lower than that for the pre-calcined powder (Degussa P25) which has a surface area of 54 m²/g. The difference between the two was mainly due to the heat treatment. According to the BDDT (Brunauer, Deming, Deming and Teller) classification, the powder and the spheres show isotherm type IV, exhibiting hysteresis loops mostly of H2 and H3. This result indicates that the composite photocatalyst contains mesopores $(2 \sim 50\ nm)$ (Sink *et al.* 1985).

Attrition resistance of TiO₂ spheres

The motion of particles in a fluidised bed reactor usually causes catalyst attrition due to the collision between particles and bed-to-wall impacts (Werther & Reppenhagen 1999). One of the main consequences of attrition is the generation of fines that are difficult to separate downstream. In order to improve the attrition resistance of the photo-catalyst, some variables could be adjusted during the synthesis process.
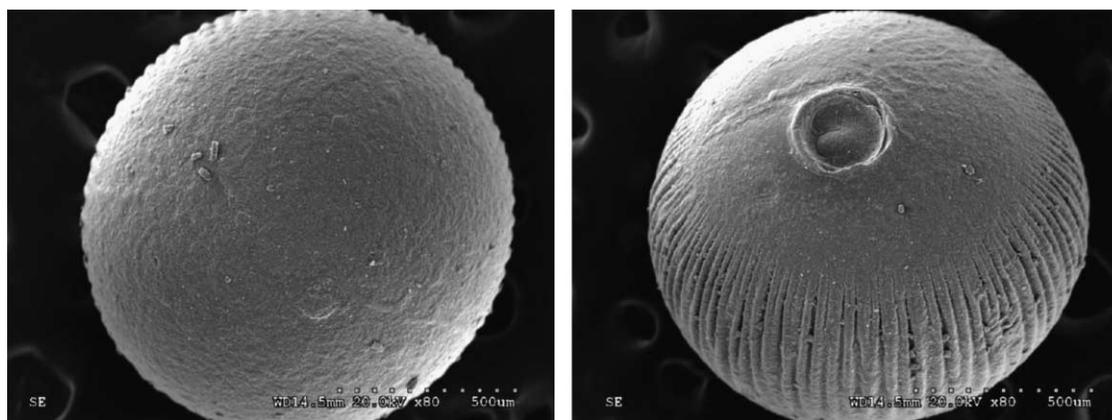

Figure 2 │ SEM micrograph of a photocatalytic sphere made of TiO₂ nanoparticles and TiO₂ commercial powder.

Hydrolysis and condensation reactions

TiO$_2$ nanoparticles are usually prepared in sol–gel process by hydrolysis and condensation reactions of titanium alkoxides to form oxopolymers which are then transformed into an oxide network. In order to obtain a homogeneous titanium oxide network, control of hydrolysis is essential (Su *et al.* 2004). Thus, the amount of water and catalyst that are mixed with the alkoxide should be carefully determined. An acid catalyst improves hydrolysis rates, also controlling the condensation rates using substoichiometric amount of water (Livage *et al.* 1988). Condensation reactions pull together the particles of the gel into a compact mass, thus building up the metal oxide crystals (Gao *et al.* 2006). Then, controlling hydrolysis and condensation reactions, this compact mass can be strengthened. The best result was obtained for the catalyst whose denatured alcohol, water, and HCl molar ratio was 1:0.9:1.3.

pH of the basic solution

The polymeric matrix had a certain viscosity needed for the spheres to be formed and also for the fast hardening of the spheres upon contact with basic solution. Because the polymeric matrix-TiO$_2$ CSG possesses a low pH, increasing the pH of the ammonia solution increases the pH difference between the two solutions, producing a harder structure that helps strengthen the TiO$_2$ spheres. An ammonia solution of 20% v/v was selected for this application.

Drying process

After preparation, the spheres are formed mainly by CSG material, which contains a significant amount of liquid. This gel must be dried before the appropriate heat treatment is applied. As the drying process proceeds, the network formed during the gelation process becomes stiffer because of the formation of new bonds due to condensation reactions (Rahaman 2007). In this research, improving the drying process allowed increasing the mechanical strength of TiO$_2$ spheres. The drying condition used for this catalysis was 80°C for 20 h.

Incorporating the aforementioned synthesis steps as well as some others along the process led to significant improvement in the level of attrition. The amount of TiO$_2$

released in the solution after 3 h of continuous operation decreased from 21 mg to 8 mg of TiO$_2$, an improvement of over 60% from the original formulation.

Photocatalytic degradation of 2,4 D

The degradation of 2,4 D was studied during 5 h in the experimental setup shown in Figure 1. As can be seen in Figure 3, a significant decrease in the amount of 2,4 D occurred under dark operation, e.g. 59% of the initial 2,4 D concentration disappeared after 30 minutes of continuous operation. Upon the start of the irradiation process, the concentration of 2,4 D decreased markedly, and more than 90% of the pollutant was degraded after 60 minutes of irradiation.

The prominent intermediate formed during the irradiation of 2,4 D solution was 2,4 Dichlorophenol (2,4 DCP). Some other minor intermediates were detected, although in a very small amount.

Model for the fluidised bed photocatalytic reactor

A complete reactor model was developed. This model was comprised of the radiation, kinetic, and fluidised bed models, which were coupled with the mass balance.

Fluidised bed model

In order to model the radiation distribution in the reactor, it was necessary to predict the plausible location of each sphere in the reactor (the reactor bed was comprised of about 10,100 spheres). A plausible arrangement of TiO$_2$ spheres was obtained using the following stochastic
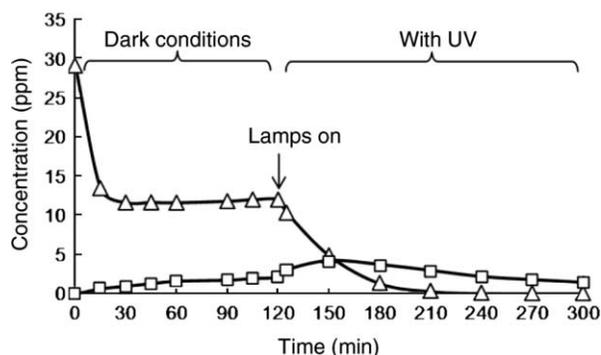
Figure 3 | Concentration of 2,4 D (△) and 2,4 DCP (□) versus time.

approach: (i) the positions of the spheres were randomly distributed without a preferential position inside the reactor volume, (ii) the distance between the centre of each sphere and the reactor walls was greater than one sphere radius, (iii) the highest position that a sphere could occupy was the top of the expanded bed (14 cm), whereas the lowest was at the bottom of the reactor, and finally, (iv) to avoid overlapping, the centres of the spheres were separated from each other by at least one sphere diameter. A matrix containing the three coordinates of the plausible location for the 10,100 spheres that comprise the reactor bed was predicted.

Radiation model

The radiative transfer equation (RTE) was solved using the Monte Carlo method and the obtained results were experimentally validated (Imoberdorf *et al.* 2008). For the Monte Carlo model, the plausible trajectories of 10^6 photons were considered. Photons were emitted uniformly from every point in the volume of the UV-lamps. Those photons that do not reach the reactor walls were considered lost, whereas those photons that reach the reactor walls (quartz tube) were partially reflected and partially transmitted (Figure 4). Photons change their direction according to the Snell law each time they enter a medium with a different refractive index. Once in the fluid phase, photons may travel without changing their direction until they reach
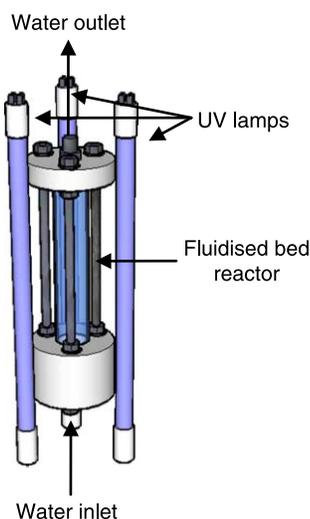
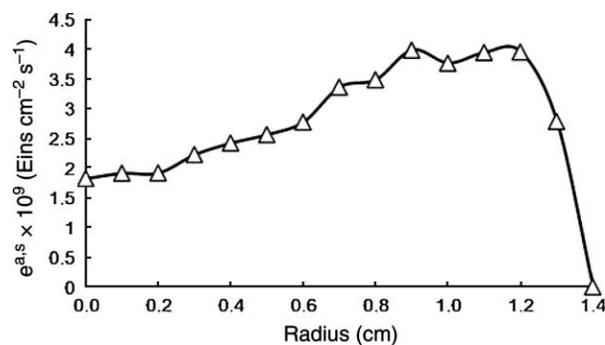**Figure 4** │ Fluidised bed photocatalytic reactor.

Figure 5 │ Radiation profiles in the reactor.

a TiO$_2$ sphere or the reactor wall. When they reach a sphere, photons may be reflected back into the fluid phase or absorbed in the TiO$_2$. The reflected photons continue their rectilinear trajectory until they reach another sphere. This sequence of events will continue until photons are absorbed in the TiO$_2$ spheres or leave the reactor without being absorbed. The local, angle-dependent reflectivity on the TiO$_2$ and quartz surfaces was calculated by using Fresnel equation. The propagation direction of those photons that have been refracted at the interface between two media was calculated using the Snell refraction law. The local superficial rate of photon absorption ($e^{a,s}$) on the surface of the TiO$_2$ spheres was calculated using the radiation model, and the obtained results are shown in Figure 5. The highest $e^{a,s}$ was obtained close to the reactor windows. The $e^{a,s}$ values reduce towards the centre of the reactor because of the attenuation effects produced by the absorption of the radiation on the TiO$_2$ spheres.

From the kinetics viewpoint, only the external surface of the spheres (A_R) was considered effective for photocatalytic reactions, since only the external area of the spheres is irradiated. The average value of the local rate of photon absorption was:

$$\langle e^{a,s} \rangle_R = \frac{\int e^{a,s}(\underline{x})\, dA_R}{A_R} = 3.29 \times 10^{-9}\, \text{Eins s}^{-1}\, \text{cm}^{-2} \tag{1}$$

Kinetic model

The kinetics of the degradation of 2,4 D is under study. According to the experimental results obtained so far, the degradation reaction rate of 2,4 D showed a dependence on the 2,4 D concentration according to the Langmuir–Hinshelwood model, and was proportional to the square

root of the rate of photon absorption. Thus, the superficial degradation rate can be expressed in terms of the local concentration of 2,4 D and the local rate of photon absorption according to:

$$r_{2,4\,D}(\underline{x}) = -\frac{k_r K C_{2,4\,D}(\underline{x})}{1 + K C_{2,4\,D}(\underline{x})} MW_{2,4\,D} \sqrt{e^{a,s}(\underline{x})} \qquad (2)$$

where k_r is the limiting rate constant of reaction at maximum coverage, K is the equilibrium constant for adsorption of the substrate onto the TiO₂, $C_{2,4\,D}$ is the local concentration of the pesticide, and $MW_{2,4\,D}$ is its molecular weight.

Mass balance

The mass balance for the system is:

$$V_{R+T}\frac{dC_{2,4\,D}}{dt} = \int r_{2,4\,D}(\underline{x})\,dA_R$$

$$= -\int \frac{k_r K C_{2,4\,D}(\underline{x})}{1 + K C_{2,4\,D}(\underline{x})} MW_{2,4\,D} \sqrt{e^{a,s}(\underline{x})}\,dA_R \qquad (3)$$

where V_{R+T} is the total volume of water in the system (i.e. the water in the tank and in the reactor), and A_R is the total external area of the photocatalytic spheres. The reactor was operated with a recycle, where the recirculation flow rate was 3.4 L/min, and the reactor volume was 86 cm³, thus the hydraulic residence time was 1.5 seconds. Under such conditions, the concentrations of the stable chemical species are expected to be uniform in the reactor, therefore:

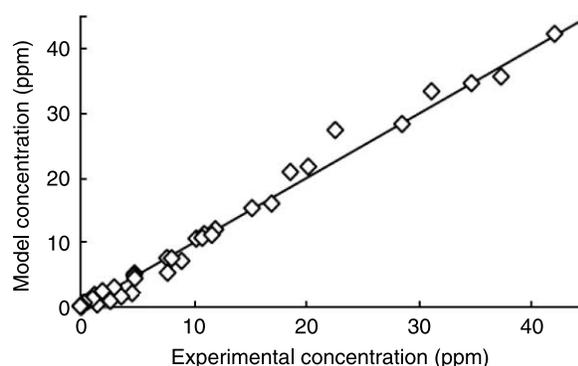$$\langle C_{2,4\,D}\rangle_R = \frac{\int C_{2,4\,D}(\underline{x})\,dV_R}{V_R} = C_{2,4\,D} \qquad (4)$$

Regarding the rate of photon absorption, the average value on the surface was considered:

$$\langle e^{a,s}\rangle_R = \frac{\int e^{a,s}(\underline{x})\,dA_R}{A_R} \qquad (5)$$

Finally, Equations (4) and (5) were substituted into Equation (3):

$$\frac{dC_{2,4\,D}}{dt} = \frac{k_r K C_{2,4\,D}}{1 + K C_{2,4\,D}} \sqrt{\langle e^{a,s}\rangle_R}\, MW_{2,4\,D}\frac{A_R}{V_{R+T}} \qquad (6)$$

The kinetic parameters were adjusted using the experimental results, the kinetic model, and the radiation model.

Figure 6 │ 2,4 D concentration for different operating conditions. Experimental values against model predicted results.

The values of the kinetic constants are as follows:

$$k_r = 1.28 \times 10^{-6}\ \text{mol cm}^{-1}\,\text{Eins}^{-0.5}\text{s}^{-0.5} \qquad (7)$$

$$K = 0.0456\ \text{L/mg} \qquad (8)$$

Experimental and model predicted concentrations for 2,4 D are compared in Figure 6. The agreement is satisfactory over the entire range of operating conditions.

CONCLUSIONS

Composite photocatalytic spheres made of TiO₂ nanoparticles and TiO₂ commercial powder were developed for application in fluidised bed photocatalytic reactors for water treatment. The main objectives were to obtain a photocatalyst with high mechanical strength and high photocatalytic activity. After optimising the synthesis variables, the TiO₂ spheres showed a high resistance to attrition. Only 0.03% of the TiO₂ was released after 3 h of continuous operation. The photocatalyst spheres possessed anatase and rutile fractions of 65% and 35%, respectively, and had a surface area of 29 m²/g. The photocatalytic activity was evaluated using 2,4 D as model pollutant. A conversion of 90% was obtained when 500 cm³ of a solution containing 30 ppm of 2,4 D was treated for 1 h in the photocatalytic reactor.

Finally, the fluidised bed photocatalytic reactor was analysed using a complete model, which was comprised of radiation, kinetic, and reactor bed hydrodynamic model components. The pollutant degradation rate showed

a dependence on 2,4 D concentration according to the Langmuir–Hinshelwood kinetic model. The reaction kinetics also showed linear relationship to square root of the rate of photon absorption.

REFERENCES

Bessekhouad, Y., Robert, D. & Weber, J. V. 2003 Synthesis of photocatalytic TiO$_2$ nanoparticles: optimization of the preparation conditions. *J. Photochem. Photobiol. A* **157**(1), 47–53.

Campanati, M., Fornasari, G. & Vaccari, A. 2003 Fundamentals in the preparation of heterogeneous catalyst. *Catal. Today* **77**, 299–314.

Eisenberg, G. 1943 Colorimetric determination of hydrogen peroxide. *Ind. Eng. Chem.* **15**(5), 327–328.

Gao, B., Ma, Y., Cao, Y., Zhao, J. & Yao, J. 2006 Effect of ultraviolet irradiation on crystallization behavior and surface microstructure of titania in the sol–gel process. *J. Solid State Chem.* **179**, 41–48.

Herrmann, J. M. 1999 Heterogenous photocatalysis: fundamentals and applications to the removal of various types of aqueous pollutants. *Catl. Today* **53**, 115–129.

Imoberdorf, G., Taghipour, F., Keshmiri, M. & Mohseni, M. 2008 Predictive radiation field modeling for fluidized bed photocatalytic reactors. *Chem. Eng. Sci.* **63**, 4228–4238.

Jackson, E. 1883 A new test for titanium and the formation of a new oxide of the metal. *Chem. News.* **47**, 157.

Livage, J. 1998 Sol–gel synthesis of heterogeneous catalyst from aqueous solutions. *Catal. Today* **41**, 3–19.

Livage, J., Henry, M. & Sanchez, C. 1988 Sol–gel chemistry of transition metal oxides. *Prog. Solid State Chem.* **18**, 259–341.

Nelson, R. J., Flakker, C. L. & Muggli, D. S. 2007 Photocatalytic oxidation of methanol using titania-based fluidized beds. *Appl. Catal. B. Environ.* **69**(3–4), 189–195.

Rahaman, M. 2007 *Ceramic Processing*. Taylor & Francis Group, USA.

Sink, K. S. W., Haul, R. A. W., Pierotti, R. A. & Siemieniewska, T. 1985 Reporting physisorption data for gas/solid systems with special reference to the determination of surface area and porosity. *Pure Appl. Chem.* **57**, 603–619.

Su, C., Hong, B.-Y. & Tseng, C.-M. 2004 Sol–gel preparation and photocatalysis of titanium dioxide. *Catal. Today* **96**, 119–126.

Wen, J. & Wilkes, G. 1996 Organic/inorganic hybrid network materials by the sol–gel approach. *Chem. Mater.* **8**, 1667–1681.

Werther, J. & Reppenhagen, J. 1999 Catalyst attrition in fluidized-bed systems. *AIChE J.* **45**(9), 2001–2010.